Journal of Cleaner Production 250 (2020) 119547

Contents lists available at ScienceDirect

Journal of Cleaner Production

journal homepage: www.elsevier.com/locate/jclepro

Eco-efficiency analysis of desalination by precipitation integrated with reverse osmosis for zero liquid discharge in oil refineries

Flávia M. Ronquim [a], Hugo M. Sakamoto [a], J.C. Mierzwa [b], Luiz Kulay [a, *], Marcelo M. Seckler [a]

[a] University of São Paulo, Department of Chemical Engineering, Av. Prof. Lineu Prestes, n. 580, 05508-010, São Paulo, SP, Brazil
[b] University of São Paulo, Department of Hydraulic and Environmental Engineering, Av. Prof. Almeida Prado, n. 83, trav. 2, 05508-900, São Paulo, SP, Brazil

ARTICLE INFO

Article history:
Received 22 April 2019
Received in revised form
10 October 2019
Accepted 2 December 2019
Available online 3 December 2019

Handling editor: Bin Chen

Keywords:
Desalination
Oil refinery wastewater
Zero liquid discharge
Precipitation integrated to reverse osmosis
Life cycle assessment
Eco-efficiency

ABSTRACT

In a process for industrial water reuse with zero liquid discharge (ZLD), a membrane separation step followed by an evaporative process is usually required. It is proposed here to maximize water conversion in the reverse osmosis (RO) membranes, in order to reduce the associated environmental impacts and economic costs from evaporative process. Considering a typical oil refinery wastewater with high inorganic scaling tendency, three ZLD virtual scenarios were proposed. A RO water recovery of 59% (default scenario SI) was increased to 89.2% with an upstream $BaSO_4$ desupersaturation step (scenario SII). A 96.3% RO water recovery (SIII) was obtained adopting also a RO intermediate softening with CaO addition and calcite seeding, as well as $MgSO_4$ dosing for additional silica removal. In all cases, the water not separated in the membrane was completely recovered in downstream evaporation and evaporative crystallization steps. A life cycle assessment (LCA) analysis suggests that the proposed scenarios enabled expressive reduction in the environmental impacts related to global warming, freshwater ecotoxicity and water consumption. Besides, it has been shown that the proposed scenarios were economically favorable. By means of an eco-efficiency analysis, economic, energetic and environmental implications appointed to benefits on developing of chemical precipitation techniques for a high RO desalting recovery in ZLD operations for aqueous effluents of petroleum refineries. It has also been found that some degree of intervention may lead to an improvement of all eco-efficiency indicators, but at some extent of intervention, at least some of the eco-efficiency indicators may become less favorable.

1. Introduction

Membrane separation processes have been extensively applied for desalination of industrial effluents, aiming to provide water of suitable quality for reuse. Electrodialysis has been utilized for over 60 years to produce desalted water from brackish water sources (Strathmann, 2010) and, more recently, membrane-distillation has been studied as a promising alternative in desalination operations (Salmón and Luis, 2018). Nowadays, reverse osmosis (RO) is the most commonly applied technology (Greenlee et al., 2009). In RO, a purified water stream and a saline concentrate stream are generated. Although the concentrate stream is often discarded in the ocean, environmental damages have been associated with such practices (Voutchkov, 2011; Watereuse Association, 2011). In order to preserve oceanic species that are sensitive to excessive salinity, regulations for effluent disposal tend to become more restrictive (Mansour et al., 2018). In desalination plants located at inland areas, concentrate disposal becomes even more problematic, since transportation to sea is economically prohibitive and discharge in rivers is often forbidden by restrictive laws (Tsai et al., 2017). Options for inland disposal of concentrate are reduced to evaporation ponds, injection into wells deeper than the groundwater and irrigation in agricultural fields (Greenlee et al., 2009). These practices, however, involve high costs with concentrate transport to disposal areas, water loss, risk of groundwater contamination and possible soil salinization (Greenlee et al., 2009; Mansour et al., 2018; Oren et al., 2010). Due to such counterproductive aspects, methods have been proposed for partial, or even full recovery of the aqueous fraction of the concentrate as reuse water (Subramani and Jacangelo, 2014). Given the high cost of concentrate disposal, Cingolani et al. (2017) identified economical profitability in

* Corresponding author.
E-mail addresses: luiz.kulay@usp.br, luiz.kulay@gmail.com (L. Kulay).

https://doi.org/10.1016/j.jclepro.2019.119547
0959-6526/

desalination of wastewater for industrial reuse when the water recovery is higher than 90%. Sometimes environmental gains associated with water recovery can offset the energy costs, especially in arid or semiarid regions, where insufficient surface water is available to industrial supply. In these cases, the full conversion of concentrate into pure water (and solid residue) by a so-called "zero liquid discharge" (ZLD) process is strongly encouraged (Bond and Veerapaneni, 2008). In this case, mostly thermal treatments such as crystallization and/or evaporation are used (Alnouri et al., 2018; Bond and Veerapaneni, 2008).

Due to the high energy cost associated with the thermal treatment of the RO concentrate, much attention has been paid to reduce its volume by improving the water recovery in the RO operation. The water recovery on RO is often limited by a high ion concentration in the byproduct compartment, where low solubility salts, such as $BaSO_4$, $CaCO_3$, $CaSO_4$, $SrSO_4$ and SiO_2, may have their solubility exceeded. When their metastable limits are overreached, they deposit on membranes pumps and pipelines, causing damage to them. Consequently, anti-scaling additives are commonly used as palliative measures (Macedonio et al., 2011). Scaling control for high water recovery, however, requires removal of potentially fouling elements upstream the RO operation (Rioyo et al., 2018). Several authors have achieved considerable high RO water recovery by adopting a precipitation process upstream the RO. Using a $BaSO_4$ desupersaturation unit integrated to a RO operation, Bremere et al. (1999) have reached a water recovery of 90% for treatment of surface water. Combining softening precipitation with a $CaSO_4$ desupersaturation unit, Rahardianto et al. (2010) have improved the recovery from 63% up to 87% for desalting of agricultural drainage water.

Intermediate softening precipitation has led to improvements in the water recovery in many applications: from 85% to 95% on surface water (Gabelich et al., 2011); 90%–98% on surface water (Rahardianto and GaoGabelichWilliamsCohen, 2007); 80–97% on municipal groundwater (Rioyo et al., 2018); 60%–90% on mining contaminated groundwater (SubramaniCryerLiuLehmanNingJacangelo, 2012) and from 90 to 97% on desert wells water (Ning et al., 2006).

A few authors have dedicated their studies exclusively to the cost's aspects of these precipitation processes prior to the RO operation. Juby et al. (2008) have estimated the costs associated to softening, reporting substantial economic impact by the chemicals applied (lime and soda ash). Sanciolo et al. (2012) have reported the economic convenience of precipitation in inland situations, where restrictions on concentrate disposal makes it necessary to reduce the volume of concentrate drained into evaporation ponds. McCool et al. (2013) have suggested that a softening step is both technically and economically feasible to a desalting recovery of 83%. Bond and Veerapaneni (2008) have found that the desalination costs and energy consumption to achieve ZLD can be significantly reduced (by 50–70% and 60–75%, respectively) through treatment of the RO concentrate for further recovery by a second application of a RO unit.

Environmental aspects related to precipitation processes prior to RO have received little attention so far. Sobhani et al. (2012) carried out an energy footprint analysis to compare coastal seawater desalting with a high-recovery groundwater treatment for ZLD (by a combination of pellet reactor for radium and hardness minimization, intermediate RO precipitation and concentrated brine crystallization). The ZLD process had lower energy footprint, operation costs and energy waste. In our previous work (Sakamoto et al., 2018) on water reuse in an oil refinery, an extensive LCA has been performed, in which environmental advantages of maximizing the RO water recovery with its integration with precipitation processes have been demonstrated. We have also found that the evaporation and crystallization steps pose a smaller environmental impact when electricity is used (mechanical recompression technology) as opposed to heat generation from burning of natural-gas (multiple-stage technology). Besides, it has been found that precipitative softening is environmentally more advantageous than a desupersaturation operation.

Investigating a RO-precipitation system like the one just mentioned (Sakamoto et al., 2019), we have found that the amount of intervention caused by the precipitation process can be of importance because of the environmental impacts associated with the production and the final destination of chemical reactants. At some degree of intervention, the advantages of a high RO recovery (and the consequent small need for water evaporation) balances the disadvantages of the additional precipitation system. In order to better decide for a suitable degree of intervention, an eco-efficiency analysis is a convenient approach, as it simultaneously addresses economic, energetic and environmental implications of processes. Such approach applied to precipitation-RO processes have not been found in the literature yet and will be addressed here. In this study, an oil refinery aqueous effluent with enough quality for discharge into a water body, but not for reuse in cooling towers is considered.

A RO operation followed by thermal operations is thus applied to enable water reuse with ZLD. As the RO process demands low energy consumption when compared to evaporative processes, enhancement on RO water recovery is proposed by integration of precipitative steps. Technological desalting scenarios have been formulated in three levels of intervention: (i) anti-scaling agent mediation only in scenario SI; (ii) addition of $BaSO_4$ seeds for desupersaturation and anti-scaling agent mediation in SII and (iii) addition of $BaSO_4$ seeds, anti-scaling agent mediation and dosing of chemicals for enhanced softening in SIII. An eco-efficiency analysis along with a life cycle assessment has been developed for the first time for precipitation processes integrated with aqueous effluent treatment in a ZLD context.

2. Methodology

2.1. Proposed scenarios

The influent to the desalting unit is the effluent of an actual oil refinery in Brazil, which contains 1922 ppm total dissolved solids (TDS, see section 2.2). This low concentration is sufficient for discharge in water bodies, but additional desalination is required for reuse as cooling water. In this concentration range, a membrane operation such as reverse osmosis or electrodialysis is usually applied. SI (Fig. 1a) represents the baseline scenario, which excludes any precipitation measure. The influent is dosed with 4.0 ppm of EDTA anti-scaling agent (*ethylenediaminetetraacetic acid*), yielding a RO water recovery of 59% to avoid scaling of $BaSO_4$, which would otherwise damage the separation equipment. The concentrate stream formed in the RO with about 4655 ppm TDS is further concentrated to 65,000 ppm in a six-stage vapor recompression (VC) evaporator, yielding additional reuse water. The resulting brine is sent to a VC crystallizer where the remaining water is recovered, and a small amount of particulate solid residue is disposed of.

In scenario SII (Fig. 1b), water recovery in the RO process is raised to 89.3% by application of a $BaSO_4$ desupersaturation step upstream the RO operation. The desupersaturator is an agitated vessel containing barium sulfate seeds in suspension. The seeds are discarded annually as a solid waste. The desupersaturator output stream receives 4.0 ppm of EDTA anti-scaling before entering the first membrane separation (RO-I) process, which operates with 75.1% water recovery. The RO-I concentrate, with 7586 ppm TDS, feeds a second reverse osmosis unit (RO-II), which water recovery is

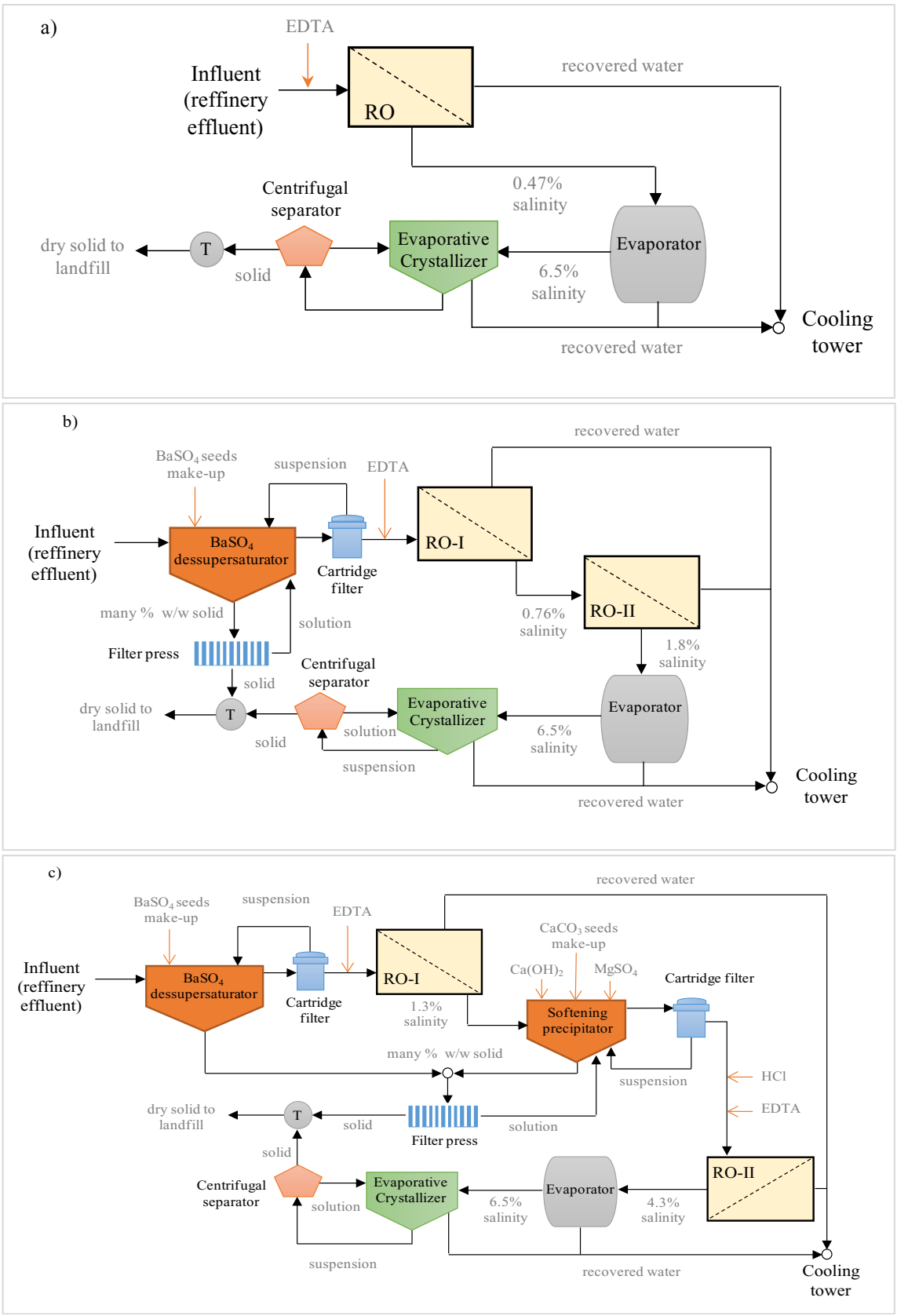

Fig. 1. Industrial water reuse with ZLD: scenarios SI (a), SII (b) and SIII (c).

Table 1
Average composition of the influent.

Analyte	Concentration(ppm)
Barium	0.60
Calcium	30.0
Strontium	2.20
Silicon	20.0
Magnesium	8.50
Sodium	625
Chloride	740
Bicarbonate	128
Potassium	20.0
Ammonium	1.71
Phosphate	4.50
Nitrate	40.0
Sulfate	300
Fluoride	0.75
TDS	1922
pH	7.50

limited to 57.2% due to the risk of silica fouling (SiO_2). The effluent (17,584 ppm) is further concentrated in a two stage VC evaporator to 65,000 ppm and thereafter in a VC crystallizer as in the SI scenario.

A water recovery of 96.3% is achieved in SIII scenario (Fig. 1c). As occurred in SII, the influent undergoes $BaSO_4$ desupersaturation and receives 4.0 ppm of EDTA before entering RO-I. The RO-I concentrate with 12,552 ppm TDS, formed at 85.0% water recovery, is submitted to softening precipitation. In this process, calcium oxide (CaO) and calcite seeds ($CaCO_3$) are mixed with the aqueous effluent in a stirred reactor to remove calcium and bicarbonate ions and also to co-precipitate barium and strontium ions, while $MgSO_4$ is dosed for removal of Si as magnesium silicate (antigorite). Seeds downstream the precipitator are decanted, filtered and recirculated.

After precipitation, the supernatant is acidified with HCl to pH = 8.0 and receives an additional 3.0 ppm dose of antifouling before entering RO-II, which operates with 75.5% water recovery. The RO-II concentrate stream with 46,093 ppm TDS is treated with VC evaporation to 65,000 ppm and VC crystallization as before.

2.2. Influent characterization

Aqueous effluents from oil refineries are typically composed of cooling tower blowdown, filter washes and rainwater precipitated over process unit areas, oil sewer, process wastewater (brine) and domestic sewage. The effluent is collected and undergoes a primary treatment for removal of suspended solids, oils and greases. Such operation consists of screens, sedimentation tanks, API separators and compressed air flotation units. The organic load is removed in a secondary treatment consisting of aeration ponds, activated sludge system, clarifiers and a stabilization pond. The resulting solution, which is the influent of this study, contains mainly dissolved inorganic salts.

The influent composition (Table 1) is taken from primary data of a Brazilian oil refinery. The TDS are calculated by summing up the contributions of all analytes shown in the Table 1 and expressed as milligram of analytes per kilogram of solution.

2.3. Desupersaturation operation

As the influent is supersaturated in relation to barium sulfate, simply seeding with $BaSO_4$ causes desupersaturation of the solution, with removal of soluble barium from aqueous matrix by crystal growth of barium sulfate upon the seed crystals. The process may be regarded as a reaction between soluble $BaCl_2$ and Na_2SO_4 to form soluble NaCl and the $BaSO_4$ salt (Equation (1)).

Table 2
Parameters of the desupersaturation unit, scenarios SII and SIII.

Flow	Unit	Value
Feed stream		
Flow rate	m^3/h	250
Dissolved Barium	ppm	0.60
$BaSO_4$ seeds	kg/h	0.024
Product stream		
Flow rate	m^3/h	250
Dissolved Barium	ppm	0.022
$BaSO_4$ seeds and precipitate	kg/h	0.269
Main equipment		
Stirred reactor with decanter	m^3	25.0
Specific energy consumption	kWh/m^3	0.065

$$BaCl_2 + Na_2SO_4 \rightarrow 2NaCl + BaSO_4\downarrow \quad (1)$$

For the influent considered in Table 1, desupersaturation allowed removal of 96% barium, considering thermodynamic equilibrium at the desupersaturator outlet. Thermodynamic modeling was performed with the OLI Studio® simulator. Equilibrium at the desupersaturator outlet has been experimentally confirmed for a seed's concentration of 10 g/L and a residence time τ = 5 min (Ronquim et al., 2018). The equipment is designed accordingly. A stirred reactor with decanter is applied as also adopted by Rahardianto et al. (2010) in $CaSO_4$ desupersaturation. The reactor is designed in such a way that the outflow is mainly liquid. Any solids leaving the reactor is retained by a cartridge filter (with micrometer particle retention) and recirculated to the reactor.

Since the Ba content in the influent is in the ppm range, the solids do not leave the reaction system frequently, so a solids residence time of one year is considered, with seeds replacement thereafter. A plate and frame filter performs the separation of the solids with complete efficiency, for disposal of dry solids in landfill. Parameters of process and equipment, as well as the energy consumption of the operation are shown in Table 2.

2.4. Softening precipitation operation

In SIII a softening precipitation step is applied with addition of calcium oxide (CaO) and magnesium sulfate ($MgSO_4$). CaO fulfills two functions: (i) it raises the pH to 11, which is suitable for silica removal (Ayoub et al., 2014; Gabelich et al., 2007; Latour et al., 2016); and, (ii) it raises the Ca^{2+} concentration to stoichiometrically match the bicarbonate content of the influent, thereby promoting precipitation of calcium carbonate ($CaCO_3$) according to Equation (2). $MgSO_4$ provides Mg^{2+} ions to remove silicon as described from the stoichiometry of Equation (3) (Latour et al., 2016). Besides the formation of $CaCO_3$ (calcite) and $Mg_{48}Si_{32}O_{80}(OH)_{64}$ (antigorite), the high pH induces the precipitation of small amounts of $Ca_5(OH)(PO_4)_3$ (hydroxyapatite) and $CaMg(CO_3)$ (dolomite) (Equations (4) and (5)).

$$1\ CaO + 1\ NaHCO_3 \rightarrow 1\ NaOH + 1\ CaCO_3\downarrow \quad (2)$$

$$48\ MgCl_2 + 48\ Ca(OH)_2 + 32\ SiO_2 + 64\ H_2O \rightarrow 80\ H_2O + 48\ CaCl_2 + 1\ Mg_{48}Si_{32}O_{80}(OH)_{64}\downarrow \quad (3)$$

$$3\ Na_3PO_4 + 5\ Ca(OH)_2 \rightarrow 9\ NaOH + 1\ Ca_5(OH)(PO_4)_3\downarrow \quad (4)$$

$$1\ MgCl_2 + 1\ CaCl_2 + 2\ NaHCO_3 \rightarrow 2\ NaCl + 2\ HCl + 1\ CaMg(CO_3)_2\downarrow \quad (5)$$

Softening precipitation allows significant removals of calcium (96%), silicon (94%), magnesium (99.9%) and carbonate (83%). Thermodynamic equilibrium is assumed at the precipitator outlet as calculated with the aid of OLI Studio® software.

Calcium carbonate incorporates foreign ions into its crystalline lattice during crystal growth, promoting further removal of impurities. Based on the equation of Doerner and Hoskins (1925), Gabelich et al. (2011) correlated the uptake of Ba^{2+} and Sr^{2+} ions with the removal of Ca^{2+} from the solution (Equation (6)).

$$log([C]_e/[C]_i) = K_c.\ log\left(\frac{[Ca^{2+}]_e}{[Ca^{2+}]_i}\right) \quad (6)$$

(C) is the molar concentrations of the ions incorporated into the $CaCO_3$ precipitated. The subscripts (e) and (i) indicate, respectively, the effluent and the influent of the precipitator. (K_C) refers to a factor of the species incorporated into the $CaCO_3$ ($K_{Ba} = 1.29$ and $K_{Sr} = 0.81$). Applying Equation (6) for the present influent, the barium and strontium removal rates of were 99% and 98%, respectively.

For softening precipitation reaction, a stirred reactor with residence time $\tau = 20$ min is considered. According to Gabelich et al. (2007) and Rahardianto and GaoGabelichWilliamsCohen (2007), calcite seeds (12.5 g/L) accelerated the depletion of supersaturation. Removal of formed solid is done continuously. As before, a plate and frame filter separates particles/liquid with complete efficiency. At the liquid outlet of the precipitator, a small quantity of solids is retained by a cartridge filter and recirculated. Table 3 summarizes the key process information.

2.5. Membranes operation

For the reverse osmosis operation, the factor (FC_i) be the ionic concentration factor for the (i^{th}) component at the concentrate stream in relation to the feed stream (Equation (7)). The parameters (C_{Ci}), (C_{Pi}) and (C_{Ai}) are the molar concentrations of compound (i) in the concentrate, permeate and in the feed stream, respectively. (R_{Si}) is the membrane rejection rate for component (i) and (R_w) refers to the water recovery of the system, defined as the ratio of the mass flows of the permeate (Q_p) and feed (Q_a) [both, expressed in (kg/h)] (Equations (8) and (9)). Using the above definitions and mass balances around the RO operation one finds the following relation:

$$FC_i = \left(C_{C_i} / C_{p_i}\right) = (1/R_w).[1 - R_w.(1 - R_{si})] \quad (7)$$

$$R_{Si} = 1 - (C_{Pi} / C_{Ai}) \quad (8)$$

$$R_w = (Q_p / Q_a) \quad (9)$$

Equation (7) shows that for a certain (R_{Si}), the concentration of a component at the concentrate stream increases with the water recovery. For a sufficiently high value of R_w, the C_{Ci} exceeds the solubility of a solid compound containing the (i) component. The solution is then said to be supersaturated with respect to this particular solid. The supersaturation ratio (S_i) described in Equation (10) expresses how far the equilibrium has been exceeded and Equation (11) provides an example of how the $BaSO_4$, supersaturation ratio (S_{BaSO_4}) is determined.

$$S_i = \sqrt{\frac{a_{i+}\ a_{i-}}{K_{ps_i}}} \quad (10)$$

$$S_{BaSO_4} = \sqrt{\frac{a_{Ba^{2+}} a_{SO_4{}^{2-}}}{K_{ps_{BaSO4}}}} = 10^3 \sqrt{\frac{\gamma_{Ba^{2+}}\ C_{C_{Ba^{2+}}}\ \gamma_{SO_4{}^{2-}}\ C_{C_{SO_4{}^{2-}}}}{K_{ps_{BaSO4}}}} \quad (11)$$

where:

a_{i+}, a_{i-}, $a_{Ba^{2+}}$ and $a_{SO_4{}^{2-}}$: activities of cation i^+, anion i^-, Ba^{2+} and SO_4^{2-} that constitute the solid compound
K_{ps_i} and $K_{ps_{BaSO4}}$: solubility product of the solid compound
$\gamma_{Ba^{2+}}$ and $\gamma_{SO_4{}^{2-}}$: activity coefficients of Ba^{2+} and SO_4^{2-} ions

Industrial practice shows that if the (S_i) value exceeds a certain value at the concentrate stream, scaling is likely to occur. Consequently, the water recovery has a maximum value that avoids scaling of each of the low solubility salts, in the present case $CaCO_3$, $CaSO_4$, $SrSO_4$, $BaSO_4$, $Ca_3(PO_4)_2$, SiO_2 and CaF_2. For $CaCO_3$, the Langelier Saturation Index (LSI) (Equation (12)) is used instead of the supersaturation ratio. According to this approach (LSI) is the difference between the measured pH of the solution and the saturation pH (pH_S):

$$LSI = pH - pH_S \quad (12)$$

Table 4 shows the empirical supersaturation limits on concentrate stream for a safe RO operation in the presence of anti-scaling agent. These values were adapted from the IMSDesign® software's database. IMSDesign® was also used to determine the maximum recovery of water in RO for each scenario. In scenario SI, the RO

Table 3
Parameters of the softening precipitation unit for SIII.

Inputs	Unit	value
Chemicals		
$Ca(OH)_2$	kg/h	19.3
$MgSO_4$	kg/h	4.31
HCl (sol 53%$_{w/w}$)	kg/h	4.10
$CaCO_3$ seeds	kg/h	0.018
Feed stream		
Flow rate	m^3/h	37.3
TDS	ppm	12,552
Barium	ppm	0.150
Calcium	ppm	199
Strontium	ppm	14.6
Silicon	ppm	131
Magnesium	ppm	56.3
Bicarbonate	ppm	814
Outputs	unit	value
Product stream		
Flow rate	m^3/h	37.3
TDS (after HCl dosing)	ppm	11,885
Barium	ppb	1.40
Calcium	ppm	7.87
Strontium	ppb	324
Silicon	ppm	8.29
Magnesium	ppb	0.062
Bicarbonate	ppm	138
Solid salts	ppm	56.1
EDTA	g/h	998
Main equipment		
Stirred reactor with decanter	m^3	14.9
Specific energy consumption	kWh/m^3	0.05

Table 4
Supersaturation ratio limit on RO concentrate stream.

Low solubility salt	Supersaturation ratio limit
$CaCO_3$ (LSI)	1.58
$CaSO_4$	2.00
$SrSO_4$	3.46
$BaSO_4$	10.0
$Ca_3(PO_4)_2$	1.55
SiO_2	1.18
CaF_2	22.3

recovery is limited to 59% in order to avoid $BaSO_4$ scaling. For SII it is possible to improve the water recovery until the SiO_2 supersaturation ratio becomes limiting, because of the low Ba content after the desupersaturation step. Since the overall recovery of SII is high, it is convenient to divide the RO operation into two stages, RO-I and RO-II, with water recoveries of 75.1% and 57.3%, respectively. Because of this the arrangement achieves an overall recovery to 89.3%.

The implementation of the softening precipitation process for removal of both barium and silica, makes SIII achieve a larger overall water recovery of 96.3%. For this situation, the partial efficiencies of RO-I and RO-II correspond to 85% and 75.5%. RO system configurations were calculated with the aid of IMSDesign® software, and the obtained design criteria (also used as input on RO simulation in the same software) are depicted in Table 5. The conception of the arrangements prioritizes low energy consumption by minimizing concentrate recirculation.

2.6. Evaporator and crystallizer

Evaporators and crystallizers are designed considering mechanical vapor compression (*VC*) as described by Darwish (1988), Lucas and Tabourier (1985) and Veza (1995). If compared to the commonly used multi-stage flash system (with natural gas burning), the (*VC*) desalination system is characterized by its equivalent energy efficiency, lower operational difficulties during water treatment (due to low operating temperatures) and, in general, lower cost per cubic meter of product (Darwish, 1988). In addition, Sakamoto et al. (2018) and Sakamoto et al. (2019) have recently suggested replacing the conventional heat source (natural gas) with one of lower environmental impact. In the (*VC*) operation this energy input consists of electricity provided by the Brazilian grid, which is mainly derived from renewable energy sources.

The evaporator is fed by the RO concentrate stream (Q_s). The vapor stream (Q_{v1}), with a negligible total dissolved solids concentration, is condensed to become reused water. For the sake of simplicity, it was assumed that the formation of solids in the evaporator would be negligible. The evaporator also yields a brine stream (Q_s) with a total dissolved solid concentration (TDS_{c1}) of 65,000 ppm. Its mass flow rate and the concentrations of each dissolved species after evaporation are calculated as described in Equations (13) and (14).

$$Q_s = Q_{v1} \cdot \frac{TDS_{c1}}{6,50} \tag{13}$$

$$X_{Si} = \left(X_{C_i} \cdot Q_C - X_{V1i} \cdot Q_{V1}\right)/Q_S \tag{14}$$

where:

X_{Si}, X_{c1i}, X_{v1i}: mass fraction of species (i) at the evaporator brine outlet, inlet and in the vapor stream (kg_i/kg sol)
Q_S, Q_{C1}: mass flows at the evaporator outlet and inlet (kg/h)
Q_{v1}: vapor mass flow rate (kg/h)

Brine from the evaporator feeds the crystallizer. Two streams are generated from this operation: a vapor flow (Q_{v2}), which becomes reused water after condensation, and a solid waste stream (Q_{R2}) that is sent to a landfill. The values of these flows can be estimated by Equations (15) and (16)

$$Q_{R2} = Q_S \cdot TDS_{c1} \tag{15}$$

$$Q_{v2} = Q_S \cdot (1 - TDS_{c1}) \tag{16}$$

Tables 6 and 7 show the main parameters of the evaporation and crystallization operations.

2.7. Life cycle assessment (LCA)

A life cycle assessment is developed to compare the environmental impacts of the proposed scenarios SI, SII and SIII for wastewater tertiary treatment with ZLD. The functional unit (FU) for each scenario is 1.0 m^3 of water for reuse as cooling tower make up. LCA is modeled with SimaPro software – v.8.3.0.0, developed by PRé Consultants®. Operational aspects and operation considered in this case are electricity, reactants consumption, transport and the final disposal of solid waste and pure water transport (from the desalting plant to the cooling tower). The environmental impacts associated to the plant construction are not considered as the equipment has a life-service of 25 years. Conversely, consumptions and emissions related to manufacture of RO membrane, are computed due, exactly due to its considerably low service life (3.3 years).

The impacts associated to energy consumption of the process were estimated in terms of Primary Energy Demand (PED) using the Cumulative Energy Demand (CED) method v. 1.09 (Frischknecht

Table 5
Parameters of RO operation.

Parameters	SI	SII		SII	
	RO-I	RO-I	RO-II	RO-I	RO-II
Feed Stream					
Flow rate (m^3/h)	250	250	62.5	250	37.5
TDS (ppm)	1922	1922	7586	1922	11,885
EDTA (ppm)	4	4	4	4	3
Permeate stream					
Flow rate (m^3/h)	147	188	35.7	212	28.1
TDS (ppm)	18.99	29.60	44.55	49.81	482.6
Concentrate stream					
Flow rate (m^3/h)	102	62.3	26.6	37.3	9.14
TDS (ppm)	4655	7586	17,584	12,552	46,093
RO design					
Concentrate recirculation (m^3/h)	–	–	–	10	40
nº of pressure vessels (1st stage)	25	34	7	32	7
nº of pressure vessels (2nd stage)	14	18	3	16	4
nº of pressure vessels (3rd stage)	–	–	–	9	–
High pressure pump (kW)	87.3	86.3	35.3	108	97.7
Specific energy consumption (kWh/m^3)	0.59	0.46	0.99	0.51	3.33

Obs.: A CPA6-LD membrane (Hydranautics - Nitto Group Company) was selected and six membrane modules are enclosed in each pressure vessel.

Table 6
Parameters of the evaporation system.

Input/Parameter	Unit	SI	SII	SIII
Feed stream				
Flow rate	m^3/h	102	26.6	9.14
TDS	ppm	4655	17,584	46,093
Temperature	°C	15.0	15.0	15.0
Distillate stream				
Flow rate	m^3/h	95.3	19.6	2.73
Brine stream				
Flow rate	m^3/h	7.09	7.03	6.41
Design				
Operating temperature	°C	62.0	62.0	62.0
Operating pressure	kPa	23.0	23.0	23.0
N° of effects	–	6	2	1
Specific energy consumption	kWh/m^3[a]	11.5	11.5	11.5
Main equipment				
Water heater	kW	2378	650	650
Evaporator (Long Tube)	m^2	7.45	1.52	212
Mechanical compressor	kW	622	450	450
Pumps for feed/distillate/brine	kW	6.96	1.82	0.63
Vacuum pump	kW	8.00	3.80	3.00

[a] Data retrieved from Lucas and Tabourier (1985) and Veza (1995).

Table 7
Parameters of the crystallization system.

Parameter	Unit	SI	SII	SIII
Feed stream				
Flow rate	m^3/h	7.09	7.03	6.41
TDS	ppm	65,000	65,000	65,000
Distillate stream				
Flow rate	m^3/h	6.87	6.80	6.22
Solid reject				
Flow rate	m^3/h	476	472	431
Design				
Evaporation temperature	°C	83.7	83.8	83.9
Operating pressure	kPa	55.0	55.0	55.0
Effects	n°.	1	1	1
Specific energy consumption	kWh/m^3	34.5	34.5	34.5
Equipment and accessories				
Water heater	kW	650.0	650	650
Heat exchangers feed (*Flat plate*)	m^2	39.5	39.1	35.7
Evaporator (*Long Tube*)	m^2	200	192	176
Mechanical compressor	kW	471	467	450
Recirculation pump	kW	59.9	46.2	43.5
Vacuum pump	kW	3.00	3.00	3.00
Centrifugal separator (diameter, Φ)	m	1.00	1.00	1.00

et al., 2007). CED takes into account the energy use along the entire life-cycle. For this purpose, in addition to direct uses of energy (i.e. electrical, thermal, mechanical and chemical), the indirect consumption of energy associated to raw materials, inputs and even construction materials are also included (Huijbregts et al., 2010). The CED concept is based on two premises. Firstly, the energy carriers (i.e. energy resources) are classified into six subcategories: three non-renewable ones: Fossil (NRF), Nuclear (NRN) and Biomass (NRB); and three renewable ones: Biomass (RB), Solar, Wind and Geothermal (RSWG) and Water (RW). Secondly, each energy carrier has an intrinsic value, which is determined by the amount of energy withdrawn from nature for its generation (Frischknecht et al., 2015). Thus, the primary energy requirement of a product or service for a certain subcategory is estimated as described in Equation (17).

$$I_i = \sum_{n=1}^{p} \left(J_n \cdot f_i^n\right) \tag{17}$$

where:

I_i: indicator of accumulated primary energy demand for subcategory (i);
J_n: total amount consumed associated to a system input n;
f_i^n : intrinsic value for the system input (n) to the subcategory (i)

Since the cumulative values of subcategory indicators are expressed on a common energy basis (e.g. MJ equivalent) it is possible to sum all these contributions in order to obtain an aggregated index (Equation (18)).

$$PED = I_{NRF} + I_{NRN} + I_{NRB} + I_{RB} + I_{RSWG} + I_{RW} \tag{18}$$

where:

PED: aggregated CED-index;
I_{NRF}, I_{NRN}, I_{NRB}, I_{RB}, I_{RSWG}, I_{RW}: indicators of primary energy demand for each subcategory

The environmental effects of Global Warming (GW) and Water Consumption (WC) were determined using the ReCiPe 2016 Midpoint (H) – v. 1.01 (Huijbregts et al., 2016), whereas the Freshwater Ecotoxicity (FEC) was estimated by the CML-IA baseline v. 3.04/EU25 (Guinée et al., 2002). The conceptual approach used by these methods is like that of CED to determine the system's primary energy requirements (Guerra et al., 2018). Therefore, the relative contribution of each input (or output) within system to the environmental load is assigned to an impact category and converted into an indicator (I_k). This is done by multiplying the cumulative contributions of such inputs (or outputs) (Y_i) over the life-cycle, by the impact factor $(IF_{i,k}^Y)$ of each substance within a certain category (k) (Equation (19)).

The impact factors express the contribution of a unit mass (1.0 kg) of a consumption (input), or emission (output) from (or to) the environment in terms of a standard substance.

$$I_k = \sum_{i=1}^{n} \left(Y_i \cdot IF_{i,k}^Y\right) \tag{19}$$

The GW effect makes use of the consolidated Global Warming Potential (GWP) indicator developed by the Intergovernmental Panel on Climate Change (Hauschild et al., 2013). For this impact, the CO_2 is defined as the standard substance. Thus, an impact factor of CH_4 to GW in $IF_{GW}^{CH4} = 30$ kg CO_{2eq} means that 1.0 kg CH_4 has the same cumulative Global Warming effect as 30 kg CO_2. According to this approach, the emissions of greenhouse gases (GHG) are quantified in terms of mass of CO_2 (e.g. kg CO_{2eq}) released into the atmosphere (Guinée et al., 2002).

Regarding WC, the method ReCiPe quantifies the use of water in the situations where this resource is evaporated, incorporated into a product, transferred to other water bodies or disposed in the sea. Overall, these consumptions are expressed in liters of water (L), which is also the standard substance for the category (Huijbregts et al., 2016). For Hauschild et al. (2013), the USETox method (Rosenbaum et al., 2008) is more advisable for situations such as the system under analysis. However, this method still meets some resistance in the community of LCA because of the absence of a consolidated methodology and of the procedures adopted to obtain characterization factors. Thus, CML was selected to evaluate FEC, and the 1,4-Dichlorobenzene (1,4-DB_{eq}) became the standard substance from which impacts in this category were expressed.

2.8. Life cycle inventory (LCI)

The influent composition (Table 1) comprises primary data from an oil refinery. In contrast, supplies of electric energy are modeled from secondary data. The electricity generation is represented by

the Brazilian matrix (BR grid) for the year 2015 (Company of Energy Research, 2016a). For that condition hydropower remained as the most expressive source of energy supply (64% of the electricity generated by the Brazilian grid). The energy from biomass (8.0%) can be represented by burning of sugarcane bagasse in a cogeneration unit that operates according to Rankine cycle. Bagasse is generated during the synthesis of sugarcane ethanol (bioethanol), of which Brazil is the main producer in the world, in amounts that goes beyond what is necessary to make distillery self-sufficient in electricity and steam. This situation, coupled with the availability of technologies for operating the Rankine cycle at high pressures (>100 bar) has enabled the generation of surplus electricity from bagasse, which has been acquired by the energy concessionaires (Company of Energy Research, 2016b). The contributions of other inputs (firewood and leaching) to this generation source are significantly lower than that of bagasse. For coal (4.0%), a mixed supply model (Brazilian and Colombian) is created considering the mining coal ore and distances of the Brazilian mines to the main thermoelectric plants (Company of Energy Research, 2016b).

For natural gas (NG) used in BR grid (13%) and for heat supply, a model – considering both the Brazilian offshore and Bolivian onshore extractions, the activities involved in refining raw natural gas, and the transport of final product – has been designed from datasets collected in Ecoinvent database, which were adapted to the local conditions (Maciel et al., 2017).

In Brazil, inland transport is carried out by diesel powered trucks. The LCI for this fuel was customized from a dataset available at the USLCI® database, also considering procedural and technological requirements practiced in Brazil. The inputs and auxiliary materials such as EDTA and barite are edited from the Ecoinvent® datasets to more closely reproduce the Brazilian reality. As occurred with diesel, the original energy inputs – electricity, NG, diesel itself and other petroleum derivatives – are replaced by inventories created specifically for this study.

For substances with no analogue LCI available in the consulted databases, the hypothesis of their generation is based on the most usual technology carried out from stoichiometric reactions with full yield ($\eta = 100\%$), and only considering utilities consumption. This is the case for hydrochloric acid (HCl) in solution, which is adapted from the anhydrous compound from the Ecoinvent database, and for the influent water, which is converted into tap water from the same database.

2.9. Cost analysis

2.9.1. Investment costs

Investment costs of equipment are estimated by the *module factor approach* (Equation (20)). Equipment specifications and assigned capacities (A) are shown in Tables 5–7 for the operation units of RO, evaporation and crystallization, respectively. The values of the parameter (A) are determined from equipment design. Data that represent K_1, K_2 and K_3 were obtained from Turton et al. (2015). The equipment cost is updated as depicted in Equation (21).

$$\log_{10} C = K_1 + K_2 \log_{10}(A) + K_3 [\log_{10}(A)]^2 \quad (20)$$

$$C_2 = C_1 \cdot \left(\frac{I_2}{I_1}\right) \quad (21)$$

The (I) parameter is the Chemical Engineering Plant Cost Index, while the subscript (1) refers to the base year of 2001, when the cost is known. Subscript (2) refers to 2017 when the cost is desired. I_1 and I_2 values are 397 and 567.5, respectively.

For some equipment, the *module factor approach* could not be applied. In these cases, the costs were obtained with the equipment supplier, based on the work of Moreira (2017). For the RO units all the elements, except the high-pressure pumps, had their costs obtained directly from suppliers: membrane modules, pressure vessels (detailed in Table 5 for each scenario) and RO cleaning system. For the evaporation and crystallization units, only the vacuum pumps costs were obtained from suppliers.

A service life of 10 years is attributed to the equipment, except for the membrane modules, with an estimated time of use of 3.3 years. Costs of plant's facilities and infrastructure are estimated from data and information obtained in literature. Therefore, the costs associated with: (i) purchased-equipment installation; (ii) instrumentation and controls (installed); (iii) piping (installed); (iv) electrical (installed); (v) engineering and supervision and (vi) construction expenses, represent 39%, 13%, 31%, 10%, 32% and 34% of the purchased equipment costs, respectively. Additional expenses with contractor's fee and contingency were expressed as 5.0% and 10% in relation to the investment costs with plant's facilities and infrastructure formerly enumerated, including purchased equipment (Peters and Timmerhaus, 1991). Finally, the scrap value of the plant, after 10 years of operation, is adopted as 10% of the purchased equipment costs. This amount is discounted from the investment's costs. Such deduction is not, however, propagated on the calculations of facilities and infrastructure costs.

2.9.2. Operating costs

Operating costs include equipment maintenance, chemical reactants, human labor, waste transportation and final disposal, and electricity (Table 8). Reactants costs are obtained from consulting with suppliers. Labor costs are calculated considering four operators, at $ 1340.38 per employee (Petrobras, 2017b), multiplied by factor $f = 1.6802$, to account for benefits and social charges (Petrobras, 2017a). The expenses related to solid waste transportation are calculated considering trucking to a landfill located 20 km from the refinery. Conversely, the transport costs of the reclaimed water are determined considering pressure drop in the stainless-steel pipe (internal diameter: $\phi_i = 193.7$ mm) which takes 250 m^3/h of treated water from the desalination plant to the cooling tower (length: L ~ 200 m).

3. Results

3.1. Environmental analysis

Table 9 presents the impacts on the Primary Energy Demand, Global Warming, Freshwater Ecotoxicity and Water Consumption for the scenarios under analysis. In general, a significant improvement is observed in the alternative scenarios (SII and SIII) compared to the baseline (SI).

Table 8
Operational costs.

Consumption goods and services	Units	Costs
Equipment maintenance[1]		6% of total cost of investment
Chemicals		
EDTA	($/ton)	2761
$BaSO_4$	($/ton)	779
$CaCO_3$	($/ton)	136
$Ca(OH)_2$	($/ton)	103
HCl (sol 53%)	($/ton)	604
$MgSO_4$	($/ton)	568
Laboratory analysis[2]	($/$m^3$)	0.20
Skilled work[3]	($/month)	9008
Final transport of solid reject	($/ton)	75.5
Final deposition of solid reject	($/ton)	302
Electricity consumption	($/kWh)	0.15

Legend: [1]Peters and Timmerhaus (1991); [2]Petrobras (2017a); [3]Cingolani et al. (2017).

Table 9
Impact profile for the scenarios SI, SII and SIII considering the production of 1.0 m^3 of reused water to a cooling tower.

Impact category	Units(/1.0 m^3 reused water)	SI	SII	SIII
PED	MJ	27.3	12.0	10.8
GW	kg CO_{2eq}	1.72	0.85	0.82
FEC	g 1,4-DB_{eq}	293	207	206
WC	L	7.68	3.88	4.93

Legend: PED: Primary Energy Demand; GW: Global Warming; FEC: Freshwater Ecotoxicity; WC: Water Consumption.

The impact on (*PED*) decreased by 56% in SII and by 60% in SIII in comparison with SI, due to the reduction in the amounts of RO concentrate to be thermally treated. The contributions of each scenario for the subcategories of *PED* are presented in Table 10. It closely resembles the impact profile of the electric grid of Brazil, since 90% of such contributions are related to electricity consumption. The participation of hydropower and thermoelectricity generated from natural gas (64% and 13%) in the Brazilian grid directly reflect the impact amounts, respectively, of Renewable, Water (RW), and Non-renewable, Fossil (NRF) obtained for each situation.

The importance of the electric power for the *PED* impact profile (SI: 98%; SII: 96% and SIII: ~90%) should be analyzed taking into account specificities of each scenario. In SIII, this utility played a somewhat smaller role because of softening precipitation, where energy is required to produce chemical reactants, particularly HCl. The acid is obtained through reaction of H_2 with Cl_2 and the hydrogen comes from steam reforming of naphtha, a process that, even using catalysts, requires extreme conditions of temperatures [760 < T(°C) < 840] and pressure [20 < P (atm) < 30] (Althaus et al., 2007). This heat supply was achieved by the burning of natural gas. According to PlasticsEurope (2005), naphtha steam reforming technology consumes 0.92 m^3 of natural gas on the production of 1.0 kg $H_{2(g)}$.

The impact on Global Warming (GW) for SII and SIII were, respectively, 51% and 52% smaller than the obtained by SI. In all scenarios, the largest source of GHG emissions was related to the plant's electricity consumption. When electricity derives from hydropower plants, the CO_2 emissions are due to the decomposition of submerged biomass as a consequence of dam formation. In the model designed for this analysis, 1.0 kWh of electricity generated from this source emits 104 g of CO_2. For thermoelectric plants the emission of GHG is related to the burning of fuel.

In SI, about 94% of the total impact on GW came from the evaporative stage electricity consumption. For the SII, the influence of electricity was reduced to 82% of the total impact due to the greater share of crystallization. In this scenario, evaporation is no longer the main energy consumer due to the high-water recovery in membrane separation. For SIII, the influence of electricity remained predominant (71%), although less intensely than in previous cases. For this arrangement, the crystallization and RO stages (due to the high volume of water recovered) were the most expressive consumers of this utility. SII and SIII also have contribution for GW in the RO stage due to the CFC-113 volatilization. After being used in the fabrication of the filter element, this organic solvent is released into the atmosphere at an average rate of 13.9 g/m^2 membrane. Finally, the obtaining of lime used in SIII emits 909 g CO_2/kg CaO as a result of $CaCO_3$ calcination.

SII and SIII also presented decreases of impact (~30%) in terms of Freshwater Ecotoxicity (FEC) compared to the result obtained by SI. For all the scenarios the contributions to this category came from the final disposal in landfill of: (i) solid salts extracted from effluent during the water recovery process, and (ii) gangue minerals generated during coal mining.

Albeit technically appropriate, the disposal of dissolved salts in refinery wastewater, especially barium chloride ($BaCl_2$), can provide adverse effects on the environment and living things. Due to its high solubility in water, of 35.8 g/100 mL at 20 °C (Kresse et al., 2007), $BaCl_2$ releases barium if exposed to slurry or other existing moisture sources in the landfill. Barium cations are mobile, spreading through underground aquifer reservoirs to plants and animals. When this heavy metal bioaccumulates in bush beans some toxicity symptoms as leaf withering, leaf growth inhibition, and complete inhibition of elongation of primary and secondary roots could be observed by Llugany et al. (2000). Evaluating Ba-induced phytotoxicity in soybean plants, Suwa et al. (2008) noted that barium accumulation in guard cells also inhibited potassium transport from epidermal cells to guard cells. Finally, Nogueira et al. (2010) showed that the growth rate and dry weight biomass of *L. sativa* (lettuce) in barium contaminated soils were significantly reduced compared to the performance of similar species cultivated in control soils. In the field of small animal practice, a commonly accepted contraindication for barium administration is the suspicion of gastrointestinal perforation, whereby Ba would exacerbate peritonitis. The potential causes of this clinical picture included existence of a foreign body, the use of nonsteroidal anti-inflammatory drugs and the suspicious pre-existing jejunal perforation with T-cell lymphoma (Ko and Mann, 2014).

Table 10
Impact profile of SI, SII and SIII per subcategory of PED.

PED Subcategory	SI	SII	SIII
(MJ/1.0 m^3 reused water)			
NRF	8.10	3.77	3.73
NRN	1.44	0.63	0.57
NRB	0.00	0.00	0.00
RB	2.27	0.98	0.86
RWSG	0.82	0.35	0.30
RW	14.7	6.31	5.38
Total	27.3	12.0	10.8

Legend: NRF: Non-renewable, Fossil; NRN: Non-renewable, Nuclear; NRB: Non-renewable, Biomass; RB: Renewable, Biomass; RWSG: Renewable, Wind, Solar, Geothermal; RW: Renewable, Water.

According to Kravchenko et al. (2014) the potential health effects of barium exposure are largely based on animal studies, while epidemiological data for humans are sparse. Anyhow, literature records in this area refer to cardiovascular and kidney diseases, metabolic, neurological, and mental disorders. The authors also warn that physiological (age, race, use of medications and transitory status, e.g. pregnancy) and behavioral (dietary patters, behavioral risks, e.g. smoking) aspects can modify such effects.

In SI the $BaCl_2$ is consequence of crystallization, whereas for SII and SIII such emission occurs in desupersaturation step. As coal is one of the energy sources of the BR grid, the tailings discarded from its mining and the ashes generated in thermoelectric plants are other important precursors of FEC. These environmental loads are more significant in the baseline scenario due to its high electrical demand.

Water consumption (WC) was reduced by 50% from SI to SII, and by 36% when the baseline scenario is compared to SIII. The performance gain of SII over SIII is related to the use of HCl. According to Althaus et al. (2007) this occurs because, one of its main raw materials [Cl_2] is produced by electrolysis requiring a large amount of cooling water (112 L/kg Cl_2).

The share of WC impacts that is common to all scenarios originates from energy consumption: SI: ~94%; SII: 82%; and SIII: 71%. In modeling, water consumption for hydropower production was disregarded, as the amount and original properties of this resource still remain intact even after its use in hydroelectric plants. The main influences observed in the scenarios were the consumption of decarbonized water for thermoelectric generation and the water

Table 11
Investment and operation costs for SI, SII and SIII: time frame: 10 years of plant operation.

Item	Costs (1000 $)		
	SI	SII	SIII
Total purchased and delivered equipments	8.346	4.588	3.829
Desupersaturation	–	557	536
RO	592	1.017	1.080
Softening precipitation	–	–	443
Evaporation	6.878	2.147	929
Crystallization	838	828	803
Centrifugal and water conveyance	38	38	38
Other investment costs	14.902	8.191	6.837
Total investment costs	23.248	12.779	10.666
Chemicals	241	243	876
Equipment maintenance	13.949	7.667	6.399
Laboratory analysis	4.307	4.307	4.307
Skilled work	1.081	1.081	1.081
Final transport and deposition of solid reject	15.788	15.646	15.156
Electricity consumption	19.084	8.255	6.728
Desupersaturation	–	215	215
RO	1.193	1.689	2.756
Softening precipitation	–	0	245
Evaporation	14.497	2.987	415
Crystallization	3.137	3.107	2.839
Centrifugal and water conveyance	258	258	258
Total operation costs	54.450	37.199	34.547
Total investment and operation costs	77.699	49.978	45.213

demand by the agrochemicals used in the production of sugarcane, which is also a source of the BR grid. Based on the findings discussed above, it can be concluded that both desupersaturation and softening precipitation applied as RO pre-treatment improved the environmental performance of the ZLD process for water reuse. This is because SII and SIII were less impacting than the baseline scenario in all impact categories analyzed in the study.

3.2. Economic analysis

The investment costs, as well as the expenses during 10 years of the desalting plant operation, are presented in Table 11 for scenarios SI to SIII. Considering total costs (investment and operation), SIII was the most economically viable scenario (with around US $ 45 million), followed by SII ($ 50 million) and by SI ($ 78 million).

When considering investment costs, a pronounced downward trend can be observed from the base scenario SI to SIII. In SIII, investment costs were the lowest (US$ 10.7 million) at 46% of SI investment, while SII investments represented 55% of SI. Although SII and SIII require additional unit operations (desupersaturation and softening precipitation) and larger RO systems, such adaptations do not generate significant expenses when compared to the savings

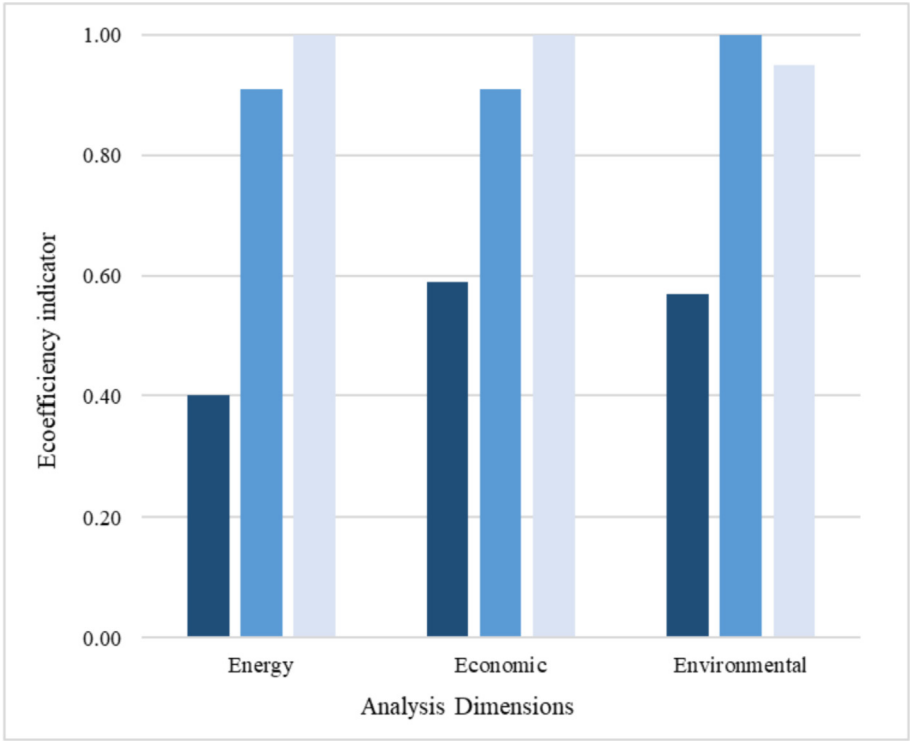

Fig. 2. Eco-efficiency indicators in the scenarios SI (■), SII (■), SIII (■).

obtained with the size reduction of the evaporation units. Such behavior is explained by the decrease on the RO concentrate volume from SI to SIII. In addition, equipment costs are propagated to other categories of investment expenditures, such as installation of equipment, instrumentation and control, piping, electrical, engineering supervision and engineering and construction expenses, as well as contractor and factor rates of contingency, further increasing the capital investment.

Operating expenses in each scenario exceeded their respective investment costs by more than twice. SIII was again the most economic scenario with US$ 34.5 million, a value 63% lower than that obtained for SI. SII follows this same trend. There are two reasons for this behavior. Firstly, the electricity consumption (especially in the evaporative treatment) decreased from SI to SII and SIII (in 57% and 65%, respectively) due to the gradual reduction in the volume of RO concentrate. Secondly, the maintenance cost of equipment also decreases from SI to SII and SIII (45% and 54%) exactly because of reduction in the equipments costs.

3.3. Eco-efficiency analysis

Eco-efficiency analysis considers three performance indicators: environmental (I_{ev}), energetic (I_{en}) and economic $(I_{\$})$. The (I_{ev}) parameter is a single indicator based on the association of the performances of a certain scenario in the different impact categories under analysis. The contribution obtained for each impact were inversely normalized: the lowest impact was set to unity, representing the best performance among the scenarios. A sum of the values ranging from 0 to 1 for GW, FEC and WC was performed and the results were directly normalized (again between 0 and 1). For (I_{en}), an inverse normalization was made between impacts of *PED*, while for $(I_{\$})$, the total cost (operational and investment) was considered on the inverse normalization.

As shown in Fig. 2, the scenarios SII and SIII were distinctively better than SI in all three performance indicators. For (I_{en}) the improved performance in SIII and SII is associated with a large proportion of water separated in the RO operations, which consume less energy (of 0.8–3.3 kg/m^3 of treated water), whereas a small amount of water is treated in the downstream evaporative processes, which consume more energy (~11.5 kW/m^3). The improvement in the $(I_{\$})$ from SI to SIII is due to an important economy in the evaporative section, whereas the additional costs of desupersaturation, softening precipitation and the membrane operations played a minor role. SII and SIII had a better (I_{ev}) than SI mainly because the reduced electricity demand reflects favorably on the GHG emission, on the freshwater contamination and on the water consumption. SIII was slightly better than SII regarding (I_{en}) and $(I_{\$})$; however, this trend is reversed in relation to (I_{ev}), mainly due to the increased impact on Water Consumption associated with the production of chemicals.

The Eco-efficiency analysis suggests that some degree of intervention may lead to an improvement of all indicators. Nevertheless, these actions should be analyzed from a wide perspective, which considers technical and process requirements apart from the environmental, energy and economic dimensions. For the current situation SIII is the most interesting option for RO assisted by precipitation in the context of ZLD treatment, if those aspects are pondered equally.

4. Conclusions

Considering a typical effluent from oil refinery, three scenarios of desalting treatment for water reuse with zero-liquid discharge were proposed. In all cases, the water was partly separated in a membrane operation, both in downstream evaporation and evaporative crystallization steps.

A RO water recovery of 59% in the standard scenario (SI) was raised to 89.2% with application of a $BaSO_4$ desupersaturation step prior to the membrane equipment (SII). With the simultaneous implementation of a pre-desupersaturation and a precipitative softening step, a 96.3% water recovery was obtained in RO (SIII). Such increases at the membranes were possible because of the added process steps removed scaling compounds that would otherwise adversely interfere with RO operations.

Life cycle assessment (LCA) has shown that the energy consumption impact (Primary Energy Demand – PED) decreased 60% from SI to SIII, due to the maximization of RO recovery, reducing the concentrate volume to be thermally treated downstream the membrane. The analysis also identified that the environmental impacts for Global Warming (GW), Freshwater Ecotoxicity (FEC) and Water Consumption (WC) decreased of 52%, 30% and 36%, respectively.

An Eco-efficiency analysis corroborates the favorable economic, energetic and environmental implications on developing of chemical precipitation techniques for a high RO desalting recovery in ZLD operations for aqueous effluents of petroleum refineries. The reductions in such dimensions were respectively of 42%, 60% and 37%. It has also been found that some degree of intervention may lead to an improvement of all eco-efficiency indicators; nevertheless, these actions should be analyzed from a wide perspective, which considers technical and process requirements.

Declaration of competing interest

None.

Acknowledgements

The authors gratefully acknowledge Petrobras for the financial support [FUSP, 2913] and the National Council for Scientific and Technological Development –CNPq for the scholarships.

References

Alnouri, S.Y., Linke, P., El-Halwagi, M.M., 2018. Accounting for central and distributed zero liquid discharge options in interplant water network design. J. Clean. Prod. 171, 644–666. https://doi.org/10.1016/j.jclepro.2017.09.236.

Althaus, H.J., Hischier, R., Osses, M., Primas, A., Hellweg, S., Jungbluth, N., Chudacoff, M., 2007. Life Cycle Inventories of Chemicals. Ecoinvent Report No. 8, V. 2.0. EMPA Dübendorf, Swiss Centre for Life Cycle Inventories, Dübendorf.

Ayoub, G.M., Zayyat, R.M., Al-Hindi, M., 2014. Precipitation softening: a pretreatment process for seawater desalination. Environ. Sci. Pollut. Res. 21, 2876–2887. https://doi.org/10.1007/s11356-013-2237-1.

Bond, R., Veerapaneni, S., 2008. Zeroing in on ZLD technologies for inland desalination. J. Am. Water Work. Assoc. 100 (9), 76–89. https://doi.org/10.1002/j.1551-8833.2008.tb09722.x.

Bremere, I., Kennedy, M., Michel, P., Van Emmerik, R., Witkamp, G.J., Schippers, J., 1999. Controlling scaling in membrane filtration systems using a desupersaturation unit. Desalination 124, 51–62. https://doi.org/10.1016/S0011-9164(99)00088-0.

Cingolani, D., Eusebi, A.L., Battistioni, P., 2017. Osmosis process for leachate treatment in industrial platform: economic and performances evaluations to zero liquid discharge. J. Environ. Manag. 203, 782–790. https://doi.org/10.1016/j.jenvman.2016.05.012.

Company of Energy Research (Empresa de Pesquisa Energética- EPE), 2016a. Balanço Brasileiro de Energia 2016 – Year 2015. EPE, Rio de Janeiro, p. 294.

Company of Energy Research (Empresa de Pesquisa Energética- EPE), 2016b. Energia Termelétrica: Gás Natural, Biomassa, Carvão. Nuclear, Rio de Janeiro, p. 417.

Darwish, M.A., 1988. Thermal analysis of vapor compression desalination system. Desalination 69, 275–295. https://doi.org/10.1016/0011-9164(88)80030-4.

Doerner, H.A., Hoskins, W.M., 1925. Co-precipitation of radium and barium sulfates. J. Am. Chem. Soc. 47, 662–675. https://doi.org/10.1021/ja01680a010.

Frischknecht, R., Jungbluth, N., Althaus, H.J., Bauer, C., Doka, G., Dones, R., Hischier, R., Hellweg, S., Humbert, S., Köllner, T., Loerincik, Y., Margni, M., Nemecek, T., 2007. Implementation of Life Cycle Assessment Methods. Ecoinvent Report No. 3, v2.0. Dübendorf, Swiss Centre for Life Cycle Inventories, p. 151.

Frischknecht, R., Wyss, F., Büsser Knöpfel, S., et al., 2015. Cumulative energy demand

in LCA: the energy harvested approach. Int. J. Life Cycle Assess. 20, 957. https://doi.org/10.1007/s11367-015-0897-4.
Gabelich, C.J., Williams, M.D., Rahardianto, A., Franklin, J.C., Cohen, Y., 2007. High-recovery reverse osmosis desalination using intermediate chemical demineralization. J. Membr. Sci. 301 (1–2), 131–141. https://doi.org/10.1016/j.memsci.2007.06.007.
Gabelich, C.J., Rahardianto, A., Northrup, C., Yun, T., Cohen, Y., 2011. Process evaluation of intermediate chemical demineralization for water recovery enhancement in production-scale brackish water desalting. Desalination 272 (1–3), 36–45. https://doi.org/10.1016/j.desal.2010.12.050.
Greenlee, L.F., Lawler, D.F., Freeman, B.D., Marrot, B., Moulin, P., 2009. Reverse osmosis desalination: water sources, technology, and today's challenges. Water Res. 43, 2317–2348. https://doi.org/10.1016/j.watres.2009.03.010.
Guerra, J.P., Cardoso, F.H., Nogueira, A., Kulay, L., 2018. Thermodynamic and environmental analysis of scaling-up cogeneration units driven by sugarcane biomass to enhance power exports. Energies 11, 73. https://doi.org/10.3390/en11010073.
Guinée, J.B., Gorrée, M., Huppes, R.H.G., Kleijn, R., Koning, A. de, Sleeswijk, L., van, O.A.W., Suh, S., Haes, H.A.U. de, Bruijn, H., de Duin, R. van, Huijbregts, M.A.J., 2002. Handbook on Life Cycle Assessment. KLUWER Academic Publisher.
Hauschild, M.Z., Goedkoop, M., Guinée, J., Heijungs, R., Huijbregts, M., Jolliet, O., Margni, M., De Schryver, A., Humbert, S., Laurent, A., Sala, S., Pant, R., 2013. Identifying best existing practice for characterization modeling in life cycle impact assessment. Int. J. Life Cycle Assess. 18, 683–697. https://doi.org/10.1007/s11367-012-0489-5.
Huijbregts, M., Hellweg, S., Frischknecht, R., Hendriks, H., Hungerbühler, K., Hendriks, A., 2010. Cumulative energy demand as predictor for the environmental burden of commodity production. Environ. Sci. Technol. 44 (6), 2189–2196. https://doi.org/10.1021/es902870s.
Huijbregts, M.A.J., Steinmann, Z.J.N., Elshout, P.M.F., Stam, G., Verones, F., Vieira, M.D.M., Hollander, A., Zijp, M., Zelm, R., 2016. ReCiPe 2016: A Harmonized Life Cycle Impact Assessment Method at Midpoint and Endpoint Level Report I: Characterization. Department of Environmental Science, Radbound University, Nijmegen, The Netherlands, p. 194.
Juby, G., Zacheis, A., Shih, W., Ravishanker, P., Mortazavi, B., Nusser, M.D., 2008. Program, Evaluation and Selection of Available Processes for a Zero-Liquid Discharge System for the Perris, California, Ground Water Basin. U.S. Department of the Interior, Bureau of Reclamation.
Ko, J.J., Mann, F.A., 2014. Barium peritonitis in small animals. J. Vet. Med. Sci. 76 (5), 621–628. https://doi.org/10.1292/jvms.13-0220.
Kravchenko, J., Darrah, T.H., Miller, R.K., Lyerly, H.K., Vengosh, A., 2014. A review of the health impacts of barium from natural and anthropogenic exposure. Environ. Geochem. Health 36 (4), 797–814. https://doi.org/10.1007/s10653-014-9622-7.
Kresse, R., Baudis, U., Jäger, P., Riechers, H.H., Wagner, H., Winkler, J., Wolf, H.U., 2007. Barium and barium compounds. In: Ullman, Franz (Ed.), Ullmann's Encyclopedia of Industrial Chemistry. Wiley-VCH. https://doi.org/10.1002/14356007.a03_325.pub2.
Latour, I., Miranda, R., Blanco, A., 2016. Optimization of silica removal with magnesium chloride in papermaking effluents: mechanistic and kinetic studies. Environ. Sci. Pollut. Res. 23, 3707–3717. https://doi.org/10.1007/s11356-015-5542-z.
Llugany, M., Poschenrieder, C., Barceló, J., 2000. Assessment of barium toxicity in bush beans. Arch. Environ. Contam. Toxicol. 39 (4), 440–444. https://doi.org/10.1007/s002440010125.
Lucas, M., Tabourier, B., 1985. The mechanical vapor compression process applied to seawater desalination: a 1,500 ton/day unit installed in the nuclear power plant of Flamanville, France. Desalination 52, 123–133. https://doi.org/10.1016/0011-9164(85)85003-7.
Macedonio, F., Katzir, L., Geisma, N., Simone, S., Drioli, E., Gilron, J., 2011. Wind-Aided Intensified eVaporation (WAIV) and Membrane Crystallizer (MCr) integrated brackish water desalination process: advantages and drawbacks. Desalination 273 (1), 127–135. https://doi.org/10.1016/j.desal.2010.12.002.
Maciel, M., Sakamoto, H., Kulay, L., 2017. Contribution to the Planning of Future Supply of Natural Gas in Brazil. VII Conferencia Internacional de Análisis de Ciclo de Vida em Latinoamérica – Medellín, pp. 195–198.
Mansour, F., Alnouri, S.Y., Al-Hindi, M., Azizi, F., Linke, P., 2018. Screening and cost assessment strategies for end-of-Pipe Zero Liquid Discharge systems. J. Clean. Prod. 179, 460–477. https://doi.org/10.1016/j.jclepro.2018.01.064.
McCool, B.C., Rahardianto, A., Faria, J.I., Cohen, Y., 2013. Evaluation of chemically-enhanced seeded precipitation of RO concentrate for high recovery desalting of high salinity brackish water. Desalination 317, 116–126. https://doi.org/10.1016/j.desal.2013.01.010.
Moreira, R.H., 2017. Desenvolvimento de um processo de reúso do efluente de refinaria baseado em sistema de osmose reversa combinado com precipitação. Polytechnic School of São Paulo, Department of Chemical Engineering São Paulo, p. 111.
Ning, R.Y., Tarquin, A., Trzcinski, M.C., Patwardhan, G., 2006. Recovery optimization of RO concentrate from desert wells. Desalination 201, 315–322. https://doi.org/10.1016/j.desal.2006.06.006.
Nogueira, T.A., Demelo, W.J., Fonseca, I.M., Marques, M.O., He, Z., 2010. Barium uptake by maize plants as affected by sewage sludge in a long-term field study. J. Hazard Mater. 181 (1–3), 1148–1157. https://doi.org/10.1016/j.jhazmat.2010.05.138.
Oren, Y., Korngold, E., Daltrophe, N., Messalem, R., Volkman, Y., Aronov, L., Weismann, M., Bouriakov, N., Glueckstern, P., Gilron, J., 2010. Pilot studies on high recovery BWRO-EDR for near zero liquid discharge approach. Desalination 261 (3), 321–330. https://doi.org/10.1016/j.desal.2010.06.010.
Peters, M.S., Timmerhaus, K.D., 1991. Plant Design and Economics for Chemical Engineers, fourth ed. McGraw Hill International Editions, New York.
Petrobras, 2017a. Edital Nº 1 - PETROBRAS/PSP RH 2017, vol. 1. http://www.cesgranrio.org.br/concursos/evento.aspx?id=petrobras0117. accessed 03 February 2018.
Petrobras, 2017b. Relatório anual. http://www.investidorpetrobras.com.br/download/6092 accessed 03 February 2018.
PlasticsEurope, 2005. Eco-profiles of the European Plastics Industry. Cracker Hydrogen, Brussels.
Rahardianto, A., Gao, J.B., Gabelich, C.J., Williams, M.D., Cohen, Y., 2007. High recovery membrane desalting of low-salinity brackish water: integration of accelerated precipitation softening with membrane RO. J. Membr. Sci. 289, 123–137. https://doi.org/10.1016/j.desal.2010.06.010.
Rahardianto, A., McCool, B.C., Cohen, Y., 2010. Accelerated desupersaturation of reverse osmosis concentrate by chemically-enhanced seeded precipitation. Desalination 264 (3), 256–267. https://doi.org/10.1016/j.desal.2010.06.018.
Rioyo, J., Aravinthan, V., Bundschuh, J., Lynch, M., 2018. Research on 'high-pH precipitation treatment' for RO concentrate minimization and salt recovery in a municipal groundwater desalination facility. Desalination 439, 168–178. https://doi.org/10.1016/j.desal.2018.04.020.
Ronquim, M.F., Cotrim, M.E.B., Guilhen, S.N., Bernardo, A., Seckler, M.M., 2018. Improved barium removal and supersaturation depletion in wastewater by precipitation with excess sulfate. J. Water. Process Eng. 23, 265–276. https://doi.org/10.1016/j.jwpe.2018.04.007.
Rosenbaum, R.K., Bachmann, T.M., Swirsky Gold, L., Huijbregts, M.A.J., Jolliet, O., Juraske, R., Koehler, A., Larsen, H.F., MacLeod, M., Margni, M., McKone, T.E., Payet, J., Schuhmacher, M., van de Meent, D., Hauschild, M.Z., 2008. USETox - the UNEP-SETAC toxicity model: recommended characterisation factors for human toxicity and freshwater ecotoxicity in Life Cycle Impact Assessment. Int. J. Life Cycle Assess. 13 (7), 532–546. https://doi.org/10.1007/s11367-008-0038-4.
Sakamoto, H.M., Ronquim, F.M., Seckler, M.M., Kulay, L.A., 2018. Study of the energetic and environmental effects of different treatment processes for water recovery: a case study on refinery oil. In: LA SDEWES – Latin America Conference of Sustainable Development of Energy, Water and Environmental Systems. SDEWES Publisher, Rio de Janeiro. Zagreb, pp. 1–13. , 1., 2018.
Sakamoto, H.M., Ronquim, F.M., Seckler, M.M., Kulay, L.A., 2019. Environmental performance of effluent conditioning systems for reuse in oil refining plants: a case study in Brazil. Energies 12, 326–339. https://doi.org/10.3390/en12020326.
Salmón, I.R., Luis, P., 2018. Membrane crystallization via membrane distillation. Chem. Eng. Process 123, 258–271.
Sanciolo, P., Ostarcevic, E., Atherton, P., Leslie, G., Fane, T., Cohen, Y., Payne, M., Gray, S., 2012. Enhancement of reverse osmosis water recovery using interstage calcium precipitation. Desalination 295, 43–52. https://doi.org/10.1016/j.desal.2012.03.015.
Sobhani, R., Abahusayn, M., Gabelich, C.J., Rosso, D., 2012. Energy Footprint analysis of brackish groundwater desalination with zero liquid discharge in inland areas of the Arabian Peninsula. Desalination 291, 106–116. https://doi.org/10.1016/j.desal.2012.01.029.
Strathmann, H., 2010. Electrodialysis, a mature technology with a multitude of new applications. Desalination 264, 268–288. https://doi.org/10.1016/j.desal.2010.04.069.
Subramani, A., Jacangelo, J.G., 2014. Treatment technologies for reverse osmosis concentrate volume minimization: a review. Separ. Purif. Technol. 122, 472–489. https://doi.org/10.1016/j.seppur.2013.12.004.
Subramani, A., Cryer, E., Liu, L., Lehman, S., Ning, R.Y., Jacangelo, J.G., 2012. Impact of intermediate concentrate softening on feed water recovery of reverse osmosis process during treatment of mining contaminated groundwater. Separ. Purif. Technol. 88, 138–145. https://doi.org/10.1016/j.seppur.2011.12.010.
Suwa, R., Jayachandran, K., Nguyen, N.T., Boulenouar, A., Fujita, K., Saneoka, H., 2008. Barium toxicity effects in soybean plants. Arch. Environ. Contam. Toxicol. 55 (3), 397–403. https://doi.org/10.1007/s00244-008-9132-7.
Tsai, J.H., Macedonio, F., Drioli, E., Giorno, L., Chou, C.Y., Hu, F.C., Li, C.L., Chuang, C.J., Tung, K.L., 2017. Membrane-based zero liquid discharge: myth or reality? J. Taiwan. Inst. Chem. Eng. 80, 192–202. https://doi.org/10.1016/j.jtice.2017.06.050.
Turton, R., Bailie, R.C., Whiting, W.B., Shaeiwitz, J.A., Bhattacharyya, D., 2015. Analysis, Synthesis and Design of Chemical Process, fourth ed. Prentice Hall, Michigan.
Veza, J.M., 1995. Mechanical vapour compression desalination plants - a case study. Desalination 101, 1–10. https://doi.org/10.1016/0011-9164(95)00002-J.
Voutchkov, N., 2011. Overview of seawater concentrate disposal alternatives. Desalination 273, 205–219. https://doi.org/10.1016/j.desal.2010.10.018.
Watereuse Association, 2011. Seawater concentrate management. White Paper. https://watereuse.org/wp-content/uploads/2015/10/Seawater_Concentrate_WP.pdf. accessed 01 February 2018.